Pathogenic LRRK2 R1441C mutation is associated with striatal alterations

Harry S. Xenias[1], Chuyu Chen[2*], Shuo Kang[2*], Bharanidharan Shanmugasundaram[2], Suraj Cherian[1], Xiaolei Situ[2], Giuseppe Scesa[2], C. Savio Chan[1#], Loukia Parisiadou[2#]

[1] Department of Physiology, Feinberg School of Medicine, Northwestern University, Chicago, IL, USA

[2] Department of Pharmacology, Feinberg School of Medicine, Northwestern University, Chicago, IL, USA

*equal contribution

[#]corresponding authors

Correspondence should be addressed to C. Savio Chan at saviochan@gmail.com or Loukia Parisiadou at loukia.parisiadou@northwestern.edu

Running title: Striatal alterations in LRRK2 knock-ins

Acknowledgments

This work was supported by Michael J. Fox Foundation for Parkinson's Research (LP), NIH R01 NS097901 (LP), R01 NS097901 (CSC), R01 NS069777 (CSC), P50 NS047085 (CSC), R01 MH112768 (CSC), R01 MH109466 (CSC), R01 NS088528 (CSC), T32 NS041234 (HSX), F32 NS098793 (HSX). We thank Brianna Berceau, Alexandria Granados, Morgan Marshall, and Nicole Curtis, for colony management and technical support. We also thank Dr. Heather Melrose for providing the LRRK2 G2019S knock-in mice.

Author contributions

HSX and SC conducted the electrophysiological measurements. HSX designed and conducted the voltammetric measurements. CC, SK, BS, XS, and GS conducted behavioral testing. HSX and SK conducted statistical analysis. LP, CSC, and HSX wrote the manuscript with input from all co-authors. LP and CSC designed, directed, and supervised the project. All authors reviewed and edited the manuscript.

Abstract (123 words)

LRRK2 mutations are associated with both familial and sporadic forms of Parkinson's disease (PD). Convergent e vidence suggests that LRRK2 plays critical roles in regulating striatal function. Here, by using knock-in mouse lines that express the two most common LRRK2 pathogenic mutations—G2019S and R1441C—we investigated how pathogenic LRRK2 mutations altered striatal physiology. We found that R1441C mice displayed a reduced nigrostriatal dopamine release and hypoexcitability in indirect-pathway striatal projection neurons. These alterations were associated with impaired striatal-dependent motor learning in the R1441C knock-in mice. In contrast, no detectable alterations were observed in the G2019S knock-in mice. In summary, our data argue that the impact of individual LRRK2 mutations cannot be simply generalized. Our findings have far-reaching implications for devising treatment strategies for PD patients.

Introduction (295 words)

The identification of LRRK2 mutations provided important insights into the genetic basis of Parkinson's disease (PD). Autosomal dominant mutations in LRRK2 are the most common genetic cause of late-onset PD to date [1, 2]. Accordingly, compelling evidence from genome-wide association studies has identified *LRRK2* as a risk factor for sporadic PD [3-5]. Patients with LRRK2 mutations exhibit clinical and pathological phenotypes that are indistinguishable from sporadic PD [6-8], suggesting common disease mechanisms. These findings urge further efforts in understanding mutant LRRK2-induced pathophysiology. The yielded knowledge about the impact of different LRRK2 mutations can be leveraged for therapeutic benefit in PD.

The LRRK2 mutations G2019S and R1441C (hereafter referred to as GS or RC) are commonly found in familial PD [9-11]. These two mutations are located in the kinase and ROC (Ras of complex GTPase) domains of the LRRK2 protein, respectively (**Figure 1a**). It is widely thought that all pathogenic mutations increase LRRK2 kinase activity [12, 13]. Recent studies show that the RC and other related mutations such as R1441G/H result in even greater activation of LRRK2 kinase activity compared to GS mutation [1, 13-15]. This highlights the importance of determining the impact associated with the RC mutation and should, in turn, facilitate the development of therapeutic innervations.

Transgenic mouse models overexpressing LRRK2 GS and RC mutations have hinted at a critical role of LRRK2 in regulating dopamine release in the striatum [16, 17]. However, as the results are highly inconsistent across studies, further efforts are needed to clarify the precise alterations induced by LRRK2 mutations. Here, by using gene-targeted knock-in (KI) mice, we systematically investigated the alterations in striatal electrochemical, electrophysiological, and motor function associated with LRRK2 RC and GS mutations.

Methods

Mice

All experiments were in compliance with Northwestern University Animal Care and Use Committee guidelines. For electrophysiological studies, Drd1a-tdTomato mice (Jackson Laboratory 016204) were crossed with R1441C mice (Jackson Laboratory 009346) [18] and Drd2-eGFP mice (MMRC 000230) were crossed with G2019S mice [19]. All mice were maintained on the C57BL/6 (Jax 000664) background. Heterozygotes for mutant LRRK2 alleles and their littermate controls, or wild-type (WT) mice, were used in all experiments. For electrophysiological recordings, hemizygotes for Drd1a-tdTomato and Drd2-eGFP were used for cellular identification. Mice were group-housed on a standard 12/12 hr light/dark cycle. Both males and females were used in this study.

Visualized *ex vivo* electrophysiology

Mice at postnatal day 90–110 were anesthetized with a ketamine-xylazine mixture and perfused transcardially with ice-cold aCSF containing the following (in mM): 125 NaCl, 2.5 KCl, 1.25 NaH_2PO_4, 2.0 $CaCl_2$, 1.0 $MgCl_2$, 25 $NaHCO_3$, and 12.5 glucose, bubbled continuously with carbogen (95% O_2 and 5% CO_2). The brains were rapidly removed, glued to the stage of a vibrating microtome (Leica Instrument), and immersed in ice-cold aCSF. Parasagittal slices containing the dorsal striatum were cut at a thickness of 240 μm and transferred to a holding chamber where they were submerged in aCSF at 37º C for 30 min and maintained at room temperature thereafter. Slices were then transferred to a small-volume (~0.5 ml) Delrin recording chamber mounted on a fixed-stage, upright microscope (Olympus). Neurons were visualized using differential interference contrast optics (Olympus), illuminated at 735 nm (Thorlabs), and imaged with a 60× water-immersion objective (Olympus) and a CCD camera

(QImaging). Genetically-defined neurons were identified by somatic eGFP or tdTomato fluorescence examined under epifluorescence microscopy with a white (6,500 K) LED (Thorlabs) and appropriate filters (Semrock).

Recordings were made at room temperature (20–22 ºC) with patch electrodes fabricated from capillary glass (Sutter Instrument) pulled on a Flaming-Brown puller (Sutter Instrument) and fire-polished with a microforge (Narishige) immediately before use. Pipette resistance was typically ~3–4 MΩ. For whole-cell current-clamp recordings, the internal solution consisted of the following (in mM): 135 $KMeSO_4$, 10 Na_2phosphocreatine, 5 KCl, 5 EGTA, 5 HEPES, 2 Mg_2ATP, 0.5 $CaCl_2$, and 0.5 Na_3GTP, with pH adjusted to 7.25–7.30 with KOH. The liquid junction potential for this internal solution was ~7 mV and was not corrected. For voltage-clamp recordings, neurons were clamped at −80 mV with an internal solution that contained the following (in mM): 125 $CsMeSO_3$, 10 Na_2-phosphocreatine, 5 HEPES, 5 tetraethylammonium chloride, 2 Mg_2ATP, 1 QX314-Cl, 0.5 Na_3GTP, 0.25 EGTA, and 0.2% (w/v) biocytin, with pH adjusted to 7.25–7.30 with CsOH. Stimulus generation and data acquisition were performed using an amplifier (Molecular Devices), a digitizer (Molecular Devices), and pClamp (Molecular Devices). For current-clamp recordings, the amplifier bridge circuit was adjusted to compensate for electrode resistance and was subsequently monitored. The signals were filtered at 1 kHz and digitized at 10 kHz. $KMeSO_4$ and Na_2-GTP were from ICN Biomedicals and Roche, respectively. All other reagents were obtained from Sigma-Aldrich.

To determine the excitability of SPNs, the frequency-current (F-I) relationship of each cell was examined with current-clamp recordings. A series of current steps beginning at −150 pA and of 500 ms duration were applied and incremented at 25 pA for each consecutive sweep. This protocol was applied until each recorded cell reached maximal firing and after entering a depolarization block. Resting membrane potential was monitored for stability and cells that varied 20% from mean baseline were excluded from the analysis.

Corticostriatal responses were recorded in voltage-clamp as previously described [20]. Electrical stimulation was performed using parallel bipolar tungsten electrodes (FHC) placed in layer 5 of the cortex. Stimulus width and intensity were adjusted via a constant current stimulator (Digitimer), to evoke a first excitatory postsynaptic current (EPSC) with an amplitude of 200–400 pA in the presence of the $GABA_A$ receptor antagonist SR95531 (10 μM). Whole-cell access was monitored with a −5 mV pulse throughout the recording. Membrane capacitance (Cm) was determined off-line as $Cm = Q_t * V_{test}$, where Qt was calculated as the integral of the transient current elicited by V_{test}, a 10 mV voltage step [21]. The paired-pulse ratio (PPR) for a given cell was calculated by taking the average of

the ratios of the second EPSC amplitude to the first EPSC amplitude for each recording sweep. Data were excluded if the series resistance of the patch pipette differed by >20% between the two recordings.

Fast-scanning cyclic voltammetry

Brain slices were prepared as described above in the electrophysiology section. Carbon fiber (7 μm diameter) (Goodfellow) electrodes were fabricated with glass capillary (Sutter) using a puller (Narishige) and fiber tips were hand-cut to 30–100 μm past the capillary tip. The carbon-fiber electrode was held at −0.4 V before each scan. A voltage ramp to and from 1.2 V (400 V/s) was delivered every 100 ms (10 Hz). Before recording, electrodes were conditioned by running the ramp at 60 Hz for 15 min and at 10 Hz for another 15 min and calibrated using 1 μM dopamine. Dopamine transients were evoked by electrical stimulation delivered through a concentric, bipolar electrode (FHC) placed in the rostrodorsal striatum (**Figure 1b**) because of its known and important involvement in reward and motivation [22-25] and motor learning and control [25-27]. A single electrical pulse (300 μA, 0.2 ms) was used [28, 29]. Data were acquired with an amplifier (Molecular Devices), a digitizer (Molecular Devices), and pClamp (Molecular Devices). For each slice, four measurements were made and then averaged. The custom analysis was written in MATLAB (MathWorks). The voltammogram and peak oxidative current amplitudes of the dopamine transient were measured. Experiments were rejected when the evoked current did not have the characteristic electrochemical signature of dopamine.

Behavioral tests

Motor learning was assessed with an accelerating rotarod in WT, RC, and GS mice. The task started when the mice were around postnatal day 60 using a rotarod apparatus (Panlab) equipped with a mouse rod (3 cm diameter) and set to 4–40 rpm acceleration over 300 s. The task consisted of eighteen daily sessions (five trials per session; intertrial-interval = 15 s, max trial duration = 300 s) divided into two phases [30]. Specifically, during the dopamine receptor antagonism phase (session 1–5), mice were systemically injected (i.p.) 30 min prior to testing with one of the following : 0.9% saline, cocktail of 1 mg/kg SCH23390 + 1 mg/kg eticlopride, 1 mg/kg SCH23390 or 1 mg/kg eticlopride. Following a 72-hr break, mice were then tested for another thirteen sessions (drug-free recovery phase).A separate cohort of WT, RC, and GS mice underwent the accelerating rotarod task for the initial

drug phase. Before the initiation of the drug-free recovery phase (after the 72-hr break), mice were assessed individually in 56 x 56 cm open-field arenas in noise-canceling boxes and illuminated by dim red lights. Session (five-minute duration) started when mice were placed in the center of the arena and locomotor activity was analyzed by the LimeLight software and reported as distance traveled.

Experimental design and statistical analyses

General graphing and statistical analyses were performed with MATLAB (MathWorks), SAS (SAS Institute), and Prism (GraphPad). Custom analysis codes are available on GitHub (https://github.com/chanlab). Sample size (n value) is defined by the number of observations (i.e., neurons, slices, or mice). No statistical method was used to predetermine the sample size. Unless noted otherwise, data are presented as median values ± median absolute deviations as measures of central tendency and statistical dispersion, respectively. Box plots are used for graphic representation of population data [31, 32]. The central line represents the median, the box edges represent the interquartile ranges, and the whiskers represent 10–90th percentiles. Normal distributions of data were not assumed for electrophysiological data. Comparisons for unrelated samples were performed using Mann–Whitney *U* test at a significance level (α) of 0.05. Unless noted otherwise, exact P values are reported. Behavioral data are presented as mean ± standard error of the mean and were analyzed with either two-way or three-way ANOVA with repeated measures followed by Tukey *post hoc* tests.

Results (1881 words)

R1441C LRRK2 mice have decreased nigrostriatal dopaminergic transmission

Studies that examine dopamine transmission in LRRK2 mutant mice have not yielded consistent results [16, 33-36]. This was in part due to the employment of bacterial artificial chromosome (BAC) or other transgenic lines confounded by unintended genomic alterations, expression of endogenous LRRK2, and unphysiological expression [37, 38]. KI mouse models serve as a well-validated approach for studying LRRK2 mutations in relevant cell types at the appropriate expression level. In this study, we used adult LRRK2 RC and GS KI mice that express mutant LRRK2 proteins under the regulation of the endogenous promoter. As there are conflicting reports on dopamine signaling in LRRK2 KI mutant mice [19, 39], we first examined nigrostriatal dopamine transmission with

135 fast-scanning cyclic voltammetry in *ex vivo* striatal tissues from WT, RC, and GS mice (**Figure 1b**). Here, we found a decrease in evoked dopamine release in RC mice compared to WT ($[DA]_{WT}$ = 856.5 ± 198.4 nM, n = 22 recordings; $[DA]_{RC}$ = 516.7 ± 148.6 nM, n = 29 recordings; p = 0.0024, Mann-Whitney U test). In addition, we found a similar decrease in evoked dopamine release in GS mice compared to WT $[DA]_{GS}$ = 562.4 ± 228.3 μM, n = 28 recordings; p = 0.0030, Mann-Whitney U test). There were no differences in evoked dopamine release between RC and GS mice
140 (p = 0.89, Mann-Whitney U test) (**Figure 1c**).

iSPNs have decreased excitability in R1441C LRRK2 mice

It is established that dopamine modulates the excitability of SPNs in naive animals [40-44]. Accordingly, the disruption of dopamine signaling profoundly alters the intrinsic properties of SPNs [20, 45]. Given our finding that
145 both RC and GS mice had decreased dopamine release, we sought to examine if direct- and indirect-pathway striatal projection neurons (dSPNs and iSPNs) have altered excitability in the LRRK2 mutant mice. Whole-cell, current-clamp recordings were performed on identified SPNs in WT, RC, and GS mice (**Figure 2**).

We found no differences in the number of spikes in dSPNs between WT and RC mice for the current (I) that elicited the half-maximum firing from dPSNs in the WT mice (I = 475 pA, $spikes_{WT}$ = 12.0 ± 4.0, n = 20 cells; $spikes_{RC}$
150 = 14.0 ± 3.0, n = 30 cells; p = 0.21, Mann–Whitney U test) (**Figure 2a**). In contrast, there was a decrease in the number of evoked spikes for the iSPNs in RC mice for the current that yielded the half-maximum firing from iSPNs in the WT mice (I = 325 pA, $spikes_{WT}$ = 14.0 ± 5.0, n_{WT} = 20 cells; $spikes_{RC}$ = 6.0 ± 6.0, n = 23 cells; p = 0.037; Mann–Whitney U test) (**Figure 2b**). To further quantify the decreased excitability in the iSPNs of RC mice, we compared the number of elicited spikes where the the frequency-current (F-I) functions for the WT and RC mice showed the
155 maximal difference (I = 625 pA). We found a decrease in the number of spikes elicited in RC mice compared to WT mice ($spikes_{WT}$ = 22.0 ± 5.0, n = 17 cells; $spikes_{RC}$ = 15.0 ± 5.0, n = 23 cells; p = 0.0010, Mann-Whitney U test) (**Figure 2b**). In contrast, we found no detectable differences in the GS mice (**Figure 2c–d**).

As the excitability of SPNs is a function of dendritic structure, we then examined possible alterations in total dendritic length by using a biophysical method [46]. Specifically, we examined whether an increase in
160 membrane capacitance (Cm) could account for the decreased excitability seen in the iSPNs of RC mice. We found

an increased membrane capacitance for iSPNs in RC mice compared to WT mice (Cm_{WT} = 68.8 ± 13.9 pF, n = 27; Cm_{RC} = 85.2 ± 13.3 pF, n = 27; p = 0.039, Mann-Whitney U Test). In contrast, no change in membrane capacitance was observed for dSPNs between RC and WT mice (Cm_{WT} = 79.4 ± 19.5 pF, n = 25; Cm_{RC} = 85.1 ± 16.0, n = 38; p = 0.98, Mann-Whitney U Test) (**Figure 2–figure supplement 1**).

The hypoexcitability of iSPNs in models of PD has been suggested as a homeostatic response to an increased corticostriatal transmission [47-49], we thus examined possible presynaptic changes in corticostriatal transmission by measuring the paired-pulse ratios (PPR) of the corticostriatal responses in WT and RC mice (see **Methods**). There were no differences in the PPRs for either dSPNs (PPR_{WT} = 1.31 ± 0.10, n = 14 cells; PPR_{RC} = 1.33 ± 0.15, n =17 cells; p = 0.18, Mann-Whitney U test) or iSPNs (PPR_{WT} = 1.28 ± 0.14, n = 13 cells; PPR_{RC} = 1.54 ± 0.25, n = 18 cells; p = 0.11, Mann-Whitney U test) (**Figure 2–figure supplement 2**). Unexpectedly, we found an increase in the 95%–5% EPSC decay time of iSPNs in RC mice compared to WT mice ($Decay_{WT}$ = 61.1 ± 38.7 ms, n = 13 cells; $Decay_{RC}$ = 139.5 ± 81.1 ms, n = 18 cells; p = 0.037, Mann-Whitney U test) (**Figure 2–figure supplement 2d**). In contrast, there were no changes in EPSC decay times for dSPNs between WT mice and RC mice ($Decay_{WT}$ = 88.7 ± 40.3 ms, n = 14 cells; $Decay_{RC}$ = 182.9 ± 136.0 ms, n = 17 cells; p = 0.13, Mann-Whitney U test) (**Figure 2–figure supplement 2e**).

R1441C mice show impaired dopamine-dependent motor learning

The dorsal striatum plays a critical role in habit and motor learning [50-53]. Given the alterations observed in the RC mice, we sought to determine if motor learning in RC mice is impaired using an accelerating rotarod task—a well-established paradigm for assessing striatally dependent motor learning [30, 54-56].

Consistent with previous studies that RC KI mice display no overt abnormalities in striatum-dependent motor learning under basal conditions [18, 57], all mice learned equally on the rotarod task in the absence of dopamine receptor antagonists (**Figure 3b**). Additionally, in agreement with prior reports [30, 54], mice treated with SCH23390 and eticlopride (dopamine D1 and D2 receptor antagonists, respectively) during the initial five-day training period showed dramatic impairment in the rotarod performance in all mice tested (session 1–5) (**Figure 3b**). Upon 72 hrs of recovery from antagonist administration, the latency to fall for WT and GS mice was increased

over subsequent sessions as compared to their corresponding saline controls (saline: n_{WT} = 10, n_{RC} = 10, and n_{GS} = 9 mice; D1 + D2 receptor antagonists: n_{WT} = 13, n_{RC} = 11, and n_{GS} = 11 mice; treatment x genotype x session interaction, $F_{102, 1887}$ = 1.95, p < 0.001, 3-way ANOVA with repeated measures) (**Figure 3b**). However, the drug-
190 treated WT and GS mice showed no difference in their latency to fall, compared to saline-treated controls over the training session (session 16–18; p > 1.0, $latency_{WT_Saline}$ vs $latency_{WT_D1+D2}$; p = 0.98, $latency_{GS_Saline}$ vs $latency_{GS_D1+D2}$, 3-way ANOVA, repeated measures) (**Figure 3b–c)**. By the end of the training session, this lack of difference in the latency to fall for both WT and GS mice remained (session 18: $latency_{WT_Saline}$ = 110 ± 29.89, n = 10; $latency_{WT_D1+D2}$ = 121 ± 21.37 p = 0.92, Mann-Whitney U test; $latency_{GS_Saline}$ = 133.34 ± 20.29, n = 8; $latency_{GS_D1+D2}$ = 79.8 ± 52.2,
195 n = 1; p = 0.15, Mann-Whitney U test) (**Figure 3b–c**, **Figure 3–table supplement 1**). In contrast, dopamine receptor antagonism unmasked a deficit in RC KI mice; they failed to reach the performance of their corresponding saline-treated controls over the training sessions (trial x genotype x drug interaction: $F_{6,116}$ = 2.24, p = 0.044; $latency_{RC_Saline}$ vs $latency_{RC_D1+D2}$, p < 0.001, 3-way ANOVA with Tukey *post hoc*) (**Figure 3c**). Similarly, they failed to reach the performance of their dopamine D1 and D2 receptor antagonist threated WT controls (trial x genotype x drug
200 interaction: $F_{6,116}$ = 2.24, p = 0.044; $latency_{WT_D1+D2}$ vs $latency_{RC_D1+D2}$, p < 0.043, 3-way ANOVA with Tukey *post hoc*) (**Figure 3c**). Additionally,to compare the performance between the saline versus dopamine receptor antagonist treated RC mice, we determined the latency to fall for each group for the final session of the trial. We found that the dopamine receptor antagonist treated mice had a decreased latency to fall compared to their saline counterparts ($Latency_{RC_saline}$ = 183 ± 26 s, n = 10; $Latency_{RC_D1+D2}$ = 64.43 ± 27.35 s, n = 11; p = 0.00015, Mann-
205 Whitney U test) (**Figure 3b–c)**.

To test if the impaired learning of RC mice was a lingering effect of the antagonist treatment, a subgroup of RC mice that received the administration of dopamine receptor antagonists were returned to their home cages without rotarod training (here referred to as "untrained mice"). After the 72-hour break, these mice were tested on the rotarod task and their performance (as measured by latency to fall) was improved compared to the RC mice
210 that underwent training in the rotarod task immediately following systemic administration of dopamine receptor antagonists (session 18: $Latency_{untrained}$ = 117.8 ± 40 s, n = 11; $Latency_{trained}$ = 64.43 ± 27.35 s, n = 11; p = 0.00050, Mann-Whitney U test) (**Figure 3d–e)**.

To examine the contributions of dopamine receptor subtype in shaping motor learning on the rotarod task, we administered D1 and D2 receptor antagonists separately during the initial acquisition. Both SCH23390 and eticlopride impaired the performance during the initial phase of the rotarod training across all genotypes (session 1–5), compared to their saline-treated controls (**Figure 3–figure supplement 1a–d**). While D1 receptor antagonism led to an immediate improvement in all genotypes in the drug-free phase (**Figure 3–figure supplement 1a–b**), D2 receptor antagonism resulted in a delayed improvement in performance (**Figure 3–figure supplement 1c–d; Figure 3–table supplement 1**). In addition, WT and GS mice treated with D2 receptor antagonist reached the performance of their saline controls by the end of the task (GS_{D2} vs GS_{saline}, p = 0.9899; WT_{D2} vs WT_{saline}, p > 1.0, 3-way ANOVA, tukey post-hoc test). In contrast, RC mice did not exhibit the performance of their saline controls across sessions (p = 0.016; 3-way ANOVA with Tukey *post hoc*). At the final session, D2 receptor antagonist treated RC mice had a reduced latency to fall compared to the saline controls (session 18, $Latency_{RC_saline}$ = 183 ± 26 s, n = 10; $Latency_{RC_D2}$ = 100.8 ± 40.6 s, n = 12; p = 0.0071, Mann-Whitney U test).

We further investigated whether the rotarod training under dopamine receptor antagonism caused impairments in the RC mice in their activity in the open field test. WT, RC, and GS mice that underwent dopamine antagonism and an initial five-day rotarod training were assessed by the total distance traveled. We found no differences between any of the groups ($Distance_{WT_Saline}$ = 28.48 ± 3.36 m; $Distance_{WT_D1+D2}$ = 24.44 ± 2.90 m; $Distance_{RC_Saline}$ = 36.02 ± 2.26 m; $Distance_{RC_D1+D2}$ = 30.62 ± 4.48 m; $Distance_{GS_Saline}$ = 31.91 ± 2.19 m; $Distance_{GS_D1+D2}$ = 30.85 ± 3.49 m; treatment effect, $F_{3,83}$ = 4.63, p = 0.0048; genotype effect, $F_{2,83}$ = 0.61, p = 0.54; treatment x genotype effect, $F_{6,83}$ = 1.94, p = 0.084, 3-way ANOVA) (**Figure 3–figure supplement 1e**). In summary, disruption of dopamine signaling during rotatord training task-specifically interferes with striatal motor learning in the RC mice, which otherwise exhibit no deficits in naturalistic behavior such as locomotion.

Discussion (734 words)

While a number of transgenic animal models have been generated to interrogate dysfunction associated with mutant LRRK2, the findings so far have been inconsistent. The most parsimonious explanation is the

differences in expression levels of mutant LRRK2 in the presence of endogenous LRRK2, as well as the different
240 promoters, used to drive the expression of mutant protein [16]. In this study, by using RC and GS KI mice that express the mutant LRRK2 protein in physiological expression patterns and levels, we observed a decrease in nigrostriatal dopamine release in both RC and GS mice. Additionally, iSPNs in the RC mice showed a selective decrease in excitability, while no differences were found in dSPNs. Consistent with previous findings [39, 49], we found no changes in the intrinsic properties of SPNs in the GS mice. The alterations in the cellular properties of SPNs were
245 paralleled with impairments in dopamine-dependent striatal motor learning in RC mice. We currently do not fully understand the dissociation between impaired dopamine release and striatal alterations; however, these data argue that additional players such as altered PKA signaling, which underlies striatal motor learning [58, 59] are involved. Notably, we showed increased synaptic PKA activities only in RC and not GS striatal synaptic fractions [15]

250 To our knowledge, this study is the first to examine evoked dopamine release from the RC KI mice. Our results are at odds with an earlier report that measured basal dopamine content in RC mice and found no changes using bulk tissue HPLC, which lacks the spatial and temporal resolution offers by fast-scanning cyclic voltammetry [18]. On the other hand, our data corroborate the finding that stimulated catecholamine release in cultured chromaffin cells of RC mice had a 50% reduction of dopamine release, [18]. The decrease of evoked dopamine
255 release could be attributed to the role of LRRK2 in regulating presynaptic vesicle release [60-63]. In particular, Lrrk2 targets downstream Rab proteins that are involved in vesicular trafficking to the plasma membrane and direct neurotransmitter release [12, 64]. In particular we recently demonstrated that RC mutation resulted in higher phosphorylation of Rab8A—a downstream LRRK2 substrate- in synaptic striatal extracts, compared to GS [15]. Overall, our results show that the RC mutation has a more profound effect on striatal physiology.

260 Previous studies that measured dopamine in GS KI mice are contradictory. Using HPLC, reduced extracellular levels of dopamine at twelve months but not six months were reported [19]. Similarly, by using amperometry Tozzi et al. reported reduced striatal dopamine levels [39]. In contrast, young mice have increased peak dopamine levels upon repeated stimulation [49]. There are several possibilities for the variability across the results including age of experimental animals, genetic backgrounds of animal lines, and heterogeneity across

striatal subregions. In the present study, Using mice at P90–P110, here we showed that GS mutation caused decreased evoked dopamine release.

Given the importance of nigrostriatal dopamine signaling in striatal motor learning, we assessed motor learning of both RC and GS KI lines using the accelerated rotarod. Consistent with previous studies, we observed no abnormalities in motor learning in LRRK2 mutants under basal conditions [18, 57]. However, we found that dopamine receptor antagonism led to motor learning deficits in the RC mice. Specifically, our data are in agreement with previous studies showing that treatment of dopamine antagonists and training of WT mice on the rotarod results in an initial delayed motor performance even after dopamine signaling is restored [30, 65]. While the performance of WT and GS mice gradually improved with training, RC mice failed to improve their motor performance. It was previously suggested that the combination of dopamine antagonists and rotarod training leads to an experience-dependent learning impairment that involves corticostriatal plasticity [30, 66, 67]. These data are of particular importance as they mirror subclinical dopaminergic dysfunction and corticostriatal alterations of the asymptomatic LRRK2 mutation carriers [68-70].

Overall, the investigation of the preclinical symptoms of dopamine and striatal dysfunctions in the mutant LRRK2 KI mice provides the framework for implementing neuroprotective therapies and developing biomarkers to detect and monitor disease progression related to LRRK2 mutations. Specifically, given the striatal alterations we observed were in the RC mutant mice, our study highlights the importance of future studies focused on the mutations of the GTPase domain and its downstream signaling targets for the development of signaling-specific neuroprotective therapies.

References

1. Alessi, D.R. and E. Sammler, *LRRK2 kinase in Parkinson's disease.* Science, 2018. **360**(6384): p. 36-37.
2. Cookson, M.R., *The role of leucine-rich repeat kinase 2 (LRRK2) in Parkinson's disease.* Nat Rev Neurosci, 2010. **11**(12): p. 791-7.
3. Satake, W., et al., *Genome-wide association study identifies common variants at four loci as genetic risk factors for Parkinson's disease.* Nat Genet, 2009. **41**(12): p. 1303-7.

4. Nalls, M.A., et al., *Large-scale meta-analysis of genome-wide association data identifies six new risk loci for Parkinson's disease.* Nat Genet, 2014. **46**(9): p. 989-93.

5. Simon-Sanchez, J., et al., *Genome-wide association study reveals genetic risk underlying Parkinson's disease.* Nat Genet, 2009. **41**(12): p. 1308-12.

6. Di Fonzo, A., et al., *Comprehensive analysis of the LRRK2 gene in sixty families with Parkinson's disease.* Eur J Hum Genet, 2006. **14**(3): p. 322-31.

7. Haugarvoll, K., et al., *Lrrk2 R1441C parkinsonism is clinically similar to sporadic Parkinson disease.* Neurology, 2008. **70**(16 Pt 2): p. 1456-60.

8. Kluss, J.H., A. Mamais, and M.R. Cookson, *LRRK2 links genetic and sporadic Parkinson's disease.* Biochem Soc Trans, 2019. **47**(2): p. 651-661.

9. Paisan-Ruiz, C., P.A. Lewis, and A.B. Singleton, *LRRK2: cause, risk, and mechanism.* J Parkinsons Dis, 2013. **3**(2): p. 85-103.

10. Dauer, W. and C.C. Ho, *The biology and pathology of the familial Parkinson's disease protein LRRK2.* Mov Disord, 2010. **25 Suppl 1**: p. S40-3.

11. Esteves, A.R., R.H. Swerdlow, and S.M. Cardoso, *LRRK2, a puzzling protein: insights into Parkinson's disease pathogenesis.* Exp Neurol, 2014. **261**: p. 206-16.

12. Steger, M., et al., *Phosphoproteomics reveals that Parkinson's disease kinase LRRK2 regulates a subset of Rab GTPases.* Elife, 2016. **5**.

13. Liu, Z., et al., *LRRK2 phosphorylates membrane-bound Rabs and is activated by GTP-bound Rab7L1 to promote recruitment to the trans-Golgi network.* Hum Mol Genet, 2018. **27**(2): p. 385-395.

14. Purlyte, E., et al., *Rab29 activation of the Parkinson's disease-associated LRRK2 kinase.* EMBO J, 2018. **37**(1): p. 1-18.

15. Chen, C., et al., *Pathway-specific deregulation of striatal excitatory synapses in LRRK2 mutations.* bioRxiv, 2020: p. 2020.01.03.894410.

16. Volta, M. and H. Melrose, *LRRK2 mouse models: dissecting the behavior, striatal neurochemistry and neurophysiology of PD pathogenesis.* Biochem Soc Trans, 2017. **45**(1): p. 113-122.

17. Xiong, Y., T.M. Dawson, and V.L. Dawson, *Models of LRRK2-Associated Parkinson's Disease.* Adv Neurobiol, 2017. **14**: p. 163-191.

18. Tong, Y., et al., *R1441C mutation in LRRK2 impairs dopaminergic neurotransmission in mice.* Proc Natl Acad Sci U S A, 2009. **106**(34): p. 14622-7.

19. Yue, M., et al., *Progressive dopaminergic alterations and mitochondrial abnormalities in LRRK2 G2019S knock-in mice.* Neurobiol Dis, 2015. **78**: p. 172-95.

20. Chan, C.S., et al., *Strain-specific regulation of striatal phenotype in Drd2-eGFP BAC transgenic mice.* J Neurosci, 2012. **32**(27): p. 9124-32.

21. Hernandez, V.M., et al., *Parvalbumin+ Neurons and Npas1+ Neurons Are Distinct Neuron Classes in the Mouse External Globus Pallidus.* J Neurosci, 2015. **35**(34): p. 11830-47.

22. Haber, S.N., et al., *Reward-related cortical inputs define a large striatal region in primates that interface with associative cortical connections, providing a substrate for incentive-based learning.* J Neurosci, 2006. **26**(32): p. 8368-76.

23. Elliott, R., et al., *Differential response patterns in the striatum and orbitofrontal cortex to financial reward in humans: a parametric functional magnetic resonance imaging study.* J Neurosci, 2003. **23**(1): p. 303-7.

24. Schultz, W., L. Tremblay, and J.R. Hollerman, *Reward processing in primate orbitofrontal cortex and basal ganglia.* Cereb Cortex, 2000. **10**(3): p. 272-84.

25. Corlett, P.R., et al., *Prediction error during retrospective revaluation of causal associations in humans: fMRI evidence in favor of an associative model of learning.* Neuron, 2004. **44**(5): p. 877-88.

26. Wickens, J.R., J.N. Reynolds, and B.I. Hyland, *Neural mechanisms of reward-related motor learning.* Curr Opin Neurobiol, 2003. **13**(6): p. 685-90.

27. McFarland, N.R. and S.N. Haber, *Convergent inputs from thalamic motor nuclei and frontal cortical areas to the dorsal striatum in the primate.* J Neurosci, 2000. **20**(10): p. 3798-813.

28. Lemos, J.C., et al., *Enhanced GABA Transmission Drives Bradykinesia Following Loss of Dopamine D2 Receptor Signaling.* Neuron, 2016. **90**(4): p. 824-38.

29. Adrover, M.F., J.H. Shin, and V.A. Alvarez, *Glutamate and dopamine transmission from midbrain dopamine neurons share similar release properties but are differentially affected by cocaine.* J Neurosci, 2014. **34**(9): p. 3183-92.

30. Beeler, J.A., et al., *A role for dopamine-mediated learning in the pathophysiology and treatment of Parkinson's disease.* Cell Rep, 2012. **2**(6): p. 1747-61.

31. Krzywinski, M. and N. Altman, *Visualizing samples with box plots.* Nat Methods, 2014. **11**(2): p. 119-20.

32. Streit, M. and N. Gehlenborg, *Bar charts and box plots.* Nat Methods, 2014. **11**(2): p. 117.

33. Li, X., et al., *Enhanced striatal dopamine transmission and motor performance with LRRK2 overexpression in mice is eliminated by familial Parkinson's disease mutation G2019S.* J Neurosci, 2010. **30**(5): p. 1788-97.

34. Li, Y., et al., *Mutant LRRK2(R1441G) BAC transgenic mice recapitulate cardinal features of Parkinson's disease.* Nat Neurosci, 2009. **12**(7): p. 826-8.

35. Ramonet, D., et al., *Dopaminergic neuronal loss, reduced neurite complexity and autophagic abnormalities in transgenic mice expressing G2019S mutant LRRK2.* PLoS One, 2011. **6**(4): p. e18568.

36. Melrose, H.L., et al., *Impaired dopaminergic neurotransmission and microtubule-associated protein tau alterations in human LRRK2 transgenic mice.* Neurobiol Dis, 2010. **40**(3): p. 503-17.

37. Beil, J., et al., *Is BAC transgenesis obsolete? State of the art in the era of designer nucleases.* J Biomed Biotechnol, 2012. **2012**: p. 308414.

38. Chaturvedi, P., et al., *Stable and reproducible transgene expression independent of proliferative or differentiated state using BAC TG-EMBED.* Gene Ther, 2018. **25**(5): p. 376-391.

39. Tozzi, A., et al., *Dopamine D2 receptor-mediated neuroprotection in a G2019S Lrrk2 genetic model of Parkinson's disease.* Cell Death Dis, 2018. **9**(2): p. 204.

40. Lahiri, A.K. and M.D. Bevan, *Dopaminergic Transmission Rapidly and Persistently Enhances Excitability of D1 Receptor-Expressing Striatal Projection Neurons.* Neuron, 2020.

41. Gerfen, C.R. and D.J. Surmeier, *Modulation of striatal projection systems by dopamine.* Annu Rev Neurosci, 2011. **34**: p. 441-66.

42. Bernard, V., E. Normand, and B. Bloch, *Phenotypical characterization of the rat striatal neurons expressing muscarinic receptor genes.* J Neurosci, 1992. **12**(9): p. 3591-600.

43. Ericsson, J., et al., *Dopamine differentially modulates the excitability of striatal neurons of the direct and indirect pathways in lamprey.* J Neurosci, 2013. **33**(18): p. 8045-54.

44. Ding, L. and D.J. Perkel, *Dopamine modulates excitability of spiny neurons in the avian basal ganglia.* J Neurosci, 2002. **22**(12): p. 5210-8.

45. Fieblinger, T., et al., *Cell type-specific plasticity of striatal projection neurons in parkinsonism and L-DOPA-induced dyskinesia.* Nat Commun, 2014. **5**: p. 5316.

46. Gertler, T.S., C.S. Chan, and D.J. Surmeier, *Dichotomous anatomical properties of adult striatal medium spiny neurons.* J Neurosci, 2008. **28**(43): p. 10814-24.

47. Beccano-Kelly, D.A., et al., *Synaptic function is modulated by LRRK2 and glutamate release is increased in cortical neurons of G2019S LRRK2 knock-in mice.* Front Cell Neurosci, 2014. **8**: p. 301.

48. Matikainen-Ankney, B.A., et al., *Altered Development of Synapse Structure and Function in Striatum Caused by Parkinson's Disease-Linked LRRK2-G2019S Mutation.* J Neurosci, 2016. **36**(27): p. 7128-41.

49. Volta, M., et al., *Initial elevations in glutamate and dopamine neurotransmission decline with age, as does exploratory behavior, in LRRK2 G2019S knock-in mice.* Elife, 2017. **6**.

50. Kupferschmidt, D.A., et al., *Parallel, but Dissociable, Processing in Discrete Corticostriatal Inputs Encodes Skill Learning.* Neuron, 2017. **96**(2): p. 476-489 e5.

51. Shiotsuki, H., et al., *A rotarod test for evaluation of motor skill learning.* J Neurosci Methods, 2010. **189**(2): p. 180-5.

52. Monville, C., E.M. Torres, and S.B. Dunnett, *Comparison of incremental and accelerating protocols of the rotarod test for the assessment of motor deficits in the 6-OHDA model.* J Neurosci Methods, 2006. **158**(2): p. 219-23.

53. Rozas, G., et al., *The overall rod performance test in the MPTP-treated-mouse model of Parkinsonism.* J Neurosci Methods, 1998. **83**(2): p. 165-75.

54. Beeler, J.A., et al., *Dopamine-dependent motor learning: insight into levodopa's long-duration response.* Ann Neurol, 2010. **67**(5): p. 639-47.

55. Yin, H.H., et al., *Dynamic reorganization of striatal circuits during the acquisition and consolidation of a skill.* Nat Neurosci, 2009. **12**(3): p. 333-41.

56. Costa, R.M., D. Cohen, and M.A. Nicolelis, *Differential corticostriatal plasticity during fast and slow motor skill learning in mice.* Curr Biol, 2004. **14**(13): p. 1124-34.

57. Giesert, F., et al., *The pathogenic LRRK2 R1441C mutation induces specific deficits modeling the prodromal phase of Parkinson's disease in the mouse.* Neurobiol Dis, 2017. **105**: p. 179-193.

58. Brandon, E.P., et al., *Defective motor behavior and neural gene expression in RIIbeta-protein kinase A mutant mice.* J Neurosci, 1998. **18**(10): p. 3639-49.

59. Kheirbek, M.A., et al., *Adenylyl cyclase type 5 contributes to corticostriatal plasticity and striatum-dependent learning.* J Neurosci, 2009. **29**(39): p. 12115-24.

60. Piccoli, G., et al., *LRRK2 controls synaptic vesicle storage and mobilization within the recycling pool.* J Neurosci, 2011. **31**(6): p. 2225-37.

61. Matta, S., et al., *LRRK2 controls an EndoA phosphorylation cycle in synaptic endocytosis.* Neuron, 2012. **75**(6): p. 1008-21.

62. Pan, P.Y., et al., *Parkinson's Disease-Associated LRRK2 Hyperactive Kinase Mutant Disrupts Synaptic Vesicle Trafficking in Ventral Midbrain Neurons.* J Neurosci, 2017. **37**(47): p. 11366-11376.

63. Nguyen, M. and D. Krainc, *LRRK2 phosphorylation of auxilin mediates synaptic defects in dopaminergic neurons from patients with Parkinson's disease.* Proc Natl Acad Sci U S A, 2018. **115**(21): p. 5576-5581.

64. Seol, W., D. Nam, and I. Son, *Rab GTPases as Physiological Substrates of LRRK2 Kinase.* Exp Neurobiol, 2019. **28**(2): p. 134-145.

65. Kang, U.J., P. Auinger, and E.I. Parkinson Study Group, *Activity enhances dopaminergic long-duration response in Parkinson disease.* Neurology, 2012. **78**(15): p. 1146-9.

66. Zhuang, X., P. Mazzoni, and U.J. Kang, *The role of neuroplasticity in dopaminergic therapy for Parkinson disease.* Nat Rev Neurol, 2013. **9**(5): p. 248-56.

67. Koranda, J.L., et al., *Chronic Nicotine Mitigates Aberrant Inhibitory Motor Learning Induced by Motor Experience under Dopamine Deficiency.* J Neurosci, 2016. **36**(19): p. 5228-40.

68. Nandhagopal, R., et al., *Progression of dopaminergic dysfunction in a LRRK2 kindred: a multitracer PET study.* Neurology, 2008. **71**(22): p. 1790-5.

69. Helmich, R.C., et al., *Reorganization of corticostriatal circuits in healthy G2019S LRRK2 carriers.* Neurology, 2015. **84**(4): p. 399-406.

70. Vilas, D., et al., *Clinical and imaging markers in premotor LRRK2 G2019S mutation carriers.* Parkinsonism Relat Disord, 2015. **21**(10): p. 1170-6.

Figure Legends

Figure 1. RC but not GS LRRK2 mice have decreased nigrostriatal dopamine release.

a. A schematic diagram of LRRK2 protein: a family of a Ras-like G-proteins with functionally distinct multi-domains, consisting of armadillo repeats (ARM), ankyrin repeats (ANK), the leucine-rich repeats (LRR), the ROC GTPase domain where the R1441C/G/H mutations reside, and the kinase domain where the G2019S mutation resides. The WD40 domain is involved in membrane binding with ARM and ANK believed to stabilize the electrostatic surfaces of the domains. **b**. Brightfield photomicrograph of a parasagittal slice with a concentric electrical electrode placed into the dorsal striatum; a carbon fiber electrode (CFE) was inserted adjacent to the stimulation site. **c**. Population data showing the peak evoked [DA] in WT, GS, and RC LRRK2 KI mice. [DA] between WT and RC mice were different (p = 0.0024, Mann-Whitney U test). The median peak evoked concentrations were: $[DA]_{WT}$ = 856.4 ± 198.4 nM (n = 22 recordings, 13 mice); $[DA]_{RC}$ = 516.7 ± 148.6 nM (n = 29 recordings, 12 mice); $[DA]_{GS}$ = 562.4 ± 228.3 nM (n = 28 recordings, 12 mice). There was no difference in evoked release between RC and GS mice (p = 0.89; Mann-Whitney U test). **d**. Representative time courses for $[DA]_e$ with corresponding cyclic voltammograms and color maps of fast-scanning cyclic voltammetry recordings. Peak evoked responses: $[DA]_{WT}$ = 1223.7 nM; $[DA]_{RC}$ = 655.1 nM; $[DA]_{GS}$ = 710.4 nM. Colormaps are normalized to the oxidation current from the WT recording.

Figure 2. iSPNs in RC LRRK2 mice have decreased excitability.

a–b. Representative whole-cell current-clamp recordings of dSPNs and iSPNs in WT and RC LRRK2 KI mice. The three injection steps shown represent the currents for the voltage responses to different current steps the first occurrence of action potentials, and the maximum firing, respectively. No differences in the F-I function were found for dSPNs between WT and RC mice at the current where the half-maximum firing occurred in the population data

(I = 475 pA, $spikes_{WT}$ = 12.0 ± 4.0, n = 20 cells, 16 slices, 10 mice; $spikes_{RC}$ = 14.0 ± 3.0, n = 30 cells, 19 slices, 14 mice; Mann–Whitney *U* test). However, for iSPNs there was a decrease of the firing response to half-maximum
450 firing current in the RC mice compared to the WT mice (I = 325 pA, $spikes_{WT}$ = 14.0 ± 5.0, n = 20 cells, 16 slice, 10 mice; $spikes_{RC}$ = 6.0 ± 6.0, n = 23 cells, 19 slices, 14 mice; p = 0.037, Mann–Whitney *U* test). The current where the maximal difference between the F-I functions for the WT and RC mice was calculated (I = 625 pA, dotted line) to compare the number of elicited spikes between the WT and RC mice. We also found a decrease in the number of spikes elicited in RC mice compared to WT mice ($spikes_{WT}$ = 22.0 ± 4.5, n = 17 cells. 16 slices, 10 mice; $spikes_{RC}$ =
455 15.0 ± 5.0, n = 23 cells, 19 slices, 14 mice; p = 0.0011; Mann-Whitney *U* test) (**b**). **c–d**. Representative whole-cell current-clamp recordings of dSPNs and iSPNs in WT and GS LRRK2 KI mice with population F-I data. For GS mice, no differences were found in the half-maximum firing responses for either dSPNs ($spikes_{WT}$ = 8.0 ± 5.0, n = 13 cells, 12 slices, 8 mice; $spikes_{GS}$ = 11.0 ± 3.0, n = 29 cells, 23 slices, 12 mice; p = 0.12, Mann-Whitney *U* test) or iSPNs ($spikes_{WT}$ = 10.5 ± 4.8, n = 20 cells, 12 slices, 8 mice; $spikes_{GS}$ = 12.0 ± 4.0, n = 28 cells, 23 slices, 12 mice; p
460 = 0.73, Mann-Whitney *U* test). F-I data are shown as mean ± standard error of the mean.

Figure 2–figure supplement 1. iSPNs have increased membrane capacitance in RC LRRK2 mice.

a. Scatter plots of membrane capacitance with medians (center line) and interquartile ranges (whiskers) for SPNs in both WT and RC LRRK2 KI mice. Membrane capacitance (Cm) of iSPNs in RC mice was greater than in WT mice
465 (Cm_{WT} = 68.8 ± 13.9 pF, n = 27 cells, 16 slices, 10 mice; Cm_{RC} = 85.2 ± 13.3 pF, n = 27 cells, 19 slices, 14 mice; p = 0.039, Mann-Whitney *U* Test). In contrast, no change in membrane capacitance was found for dSPNs between RC and WT mice (Cm_{WT} = 79.4 ± 19.5 pF, n = 25 cells, 16 slices, 10 mice; Cm_{RC} = 85.1 ± 16.0 pF, n = 38 cells, 19 slices, 14 mice; p = 0.98, Mann-Whitney *U* Test).

470 **Figure 2–figure supplement 2. Paired-pulse ratio and 95%–5% decay time analysis.**

a. Representative brightfield photomicrograph of a WT dSPN in a parasagittal slice being recorded in voltage-clamp and held at −80 mV. **b**. High magnified fluorescent photomicrograph of the same dSPN in the panel to the left. Pipette dye loading of Alexa Fluor 647 into the cell for visualization was performed with in vivo confocal

imaging after recording. SPNs were identified by size and large number of dendritic spines, characteristic of SPNs. Inset: magnified view of boxed region showing a dendritic segment that is heavily decorated with spines. **c**. *Top left*: Mean voltage-clamp recording of the dSPN shown in **b** above. Paired-pulse stimulation of the cortex at 20 Hz elicited a pair of excitatory postsynaptic currents (EPSC). *Bottom left*: Magnified view of the amplitude decay of the second EPSC shown in the boxed region above. The red portion of the mean trace depicts the 95%–5% decay time. **d**. Population means of paired-pulse ratios of SPNs from age-matched WT and RC mice. No differences were found in either dSPNs (PPR_{WT} = 1.31 ± 0.10, n = 14 cells, 9 slices, 8 mice; PPR_{RC} = 1.33 ± 0.15, n =17 cells, 15 slices, 16 mice; p = 0.18, Mann-Whitney U test) or iSPNs (PPR_{WT} = 1.28 ± 0.14, n = 13 cells, 9 slices, 8 mice; PPR_{RC} = 1.54 ± 0.25, n = 18 cells, 15 slices, 12 mice; p = 0.11, Mann-Whitney U test). **e**. Population means of the 95%–5% decay times of SPNs from age-matched WT and RC mice. A decrease in the 95%–5% decay times in the iSPNs of RC mice compared to WT was revealed ($Decay_{WT}$ = 61.1 ± 38.7 ms, n = 13 cells, 9 slices, 8 mice; $Decay_{RC}$ = 139.5 ± 81.1 ms, n = 18 cells, 15 slices, 16 mice; p = 0.036; Mann-Whitney U test). For dSPNs, no differences were found ($Decay_{WT}$ = 88.7 ± 40.3, n = 14 cells, 10 slices, 8 mice; $Decay_{RC}$ = 182.9 ± 136.0 ms, n = 17 cells, 15 slices, 14 mice; p = 0.13, Mann-Whitney U test).

Figure 3. RC KI mice show dopamine-dependent motor learning impairments.

a. Schematic of the rotarod training paradigm. Mice were assessed over a total of 18 daily sessions where every daily session consisted of five trials. WT, GS, and RC mice were administered either saline or a cocktail of D1 receptor (SCH23390) and D2 receptor (eticlopride), 1 mg/kg of each antagonist 30 min prior to daily sessions, and trained for five successive days in an accelerated rotarod. After a 72 h break, the mice were returned to the rotarod for an additional 13 days of a drug-free recovery phase. **b**. Genotype-dependent effect of blocking both D1 and D2 receptors, during the first five sessions on rotarod performance of WT, RC, and GS mice. The average latency in the early (session 6–8) and late (session 16–18) stage in the drug-free recovery phase in **b** is summarized in **c**. Open and filled bars represent the average performance of saline control and drug-treated mice, respectively (saline treated groups: n_{WT} = 10, n_{RC} = 10, and n_{GS} = 9 mice; D1 + D2 receptor antagonist treated groups: n_{WT} = 13, n_{RC} = 11, and n_{GS} = 11 mice; *** p < 0.001 vs genotype-matched saline control). **c–d**. Improved performance of RC

500 mice (n = 10) received antagonist cocktail but no training during the first five sessions. The RC_{D1+D2} group data is from **3b–c** for reference.

Figure 3–figure supplement 1. Effect of D1 or D2 antagonism on dopamine-dependent motor learning. Rotarod performance of WT, RC, and GS mice that were administered antagonist for either D1 (SCH23390) (**a–b**)
505 or D2 receptors (eticlopride) (**c–d**), 30 min prior to training for the first five days. Solid traces are saline control plotted in **Figure 3b** for reference. **b and d**. Averaged latency of saline control (open bars) and drug-treated mice (filled bars). Early and late refer to session 6–8 and 16–18, respectively, of the no drug recovery phase (D1R antagonist treated groups: n_{WT} = 11, n_{RC} = 11, and n_{GS} = 9 mice; D2R antagonist treated groups: n_{WT} = 9, n_{RC} = 14, and n_{GS} = 10 mice; *** $p < 0.001$, ** $p < 0.01$ vs genotype-matched saline control). **e.** Distance travelled in the open
510 field after five days of rotarod training and dopamine receptor antagonist cocktail. Another group of mice received dopamine antagonist treatment and rotarod training for five days under the same schedule described in **a–d** and **Figure 3b–c**, and were tested in the open field immediately after the 72-hr break instead of the drug-free phase (saline treated groups: n_{WT} = 11, n_{RC} = 8, and n_{GS} = 7 mice; D1R + D2R antagonist treated groups: n_{WT} = 7, n_{RC} = 6, and n_{GS} = 6 mice; D1R antagonist treated groups: n_{WT} = 7, n_{RC} = 9, and n_{GS} = 9 mice; D2R antagonist treated groups:
515 n_{WT} = 8, n_{RC} = 11, and n_{GS} =7 mice).

Figure 3–table supplement 1. Summary of differences between mutants and pharmacological conditions. Summary table of *p*-values for within-treatment and within-genotype *post hoc* comparisons for both the early and late sessions during the drug-free recovery phase

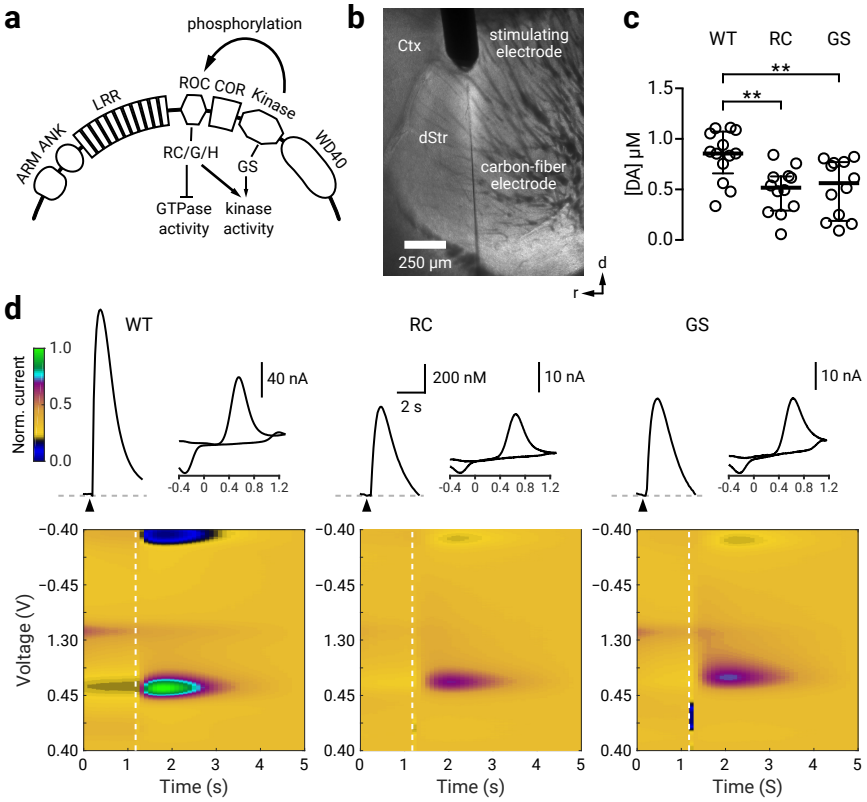
a
phosphorylation
ROC
COR
Kinase
LRR
ARM
ANK
WD40
RC/G/H
GS
GTPase activity
kinase activity
b
Ctx
stimulating electrode
dStr
carbon-fiber electrode
250 µm
d
r
c
WT
RC
GS
**
**
[DA] µM
1.5
1.0
0.5
0.0
d
WT
RC
GS
Norm. current
1.0
0.5
0.0
40 nA
200 nM
2 s
10 nA
10 nA
-0.4 0 0.4 0.8 1.2
Voltage (V)
−0.40
−0.45
1.30
0.45
0.40
0 1 2 3 4 5
Time (s)
Time (s)
Time (S)

Figure 1

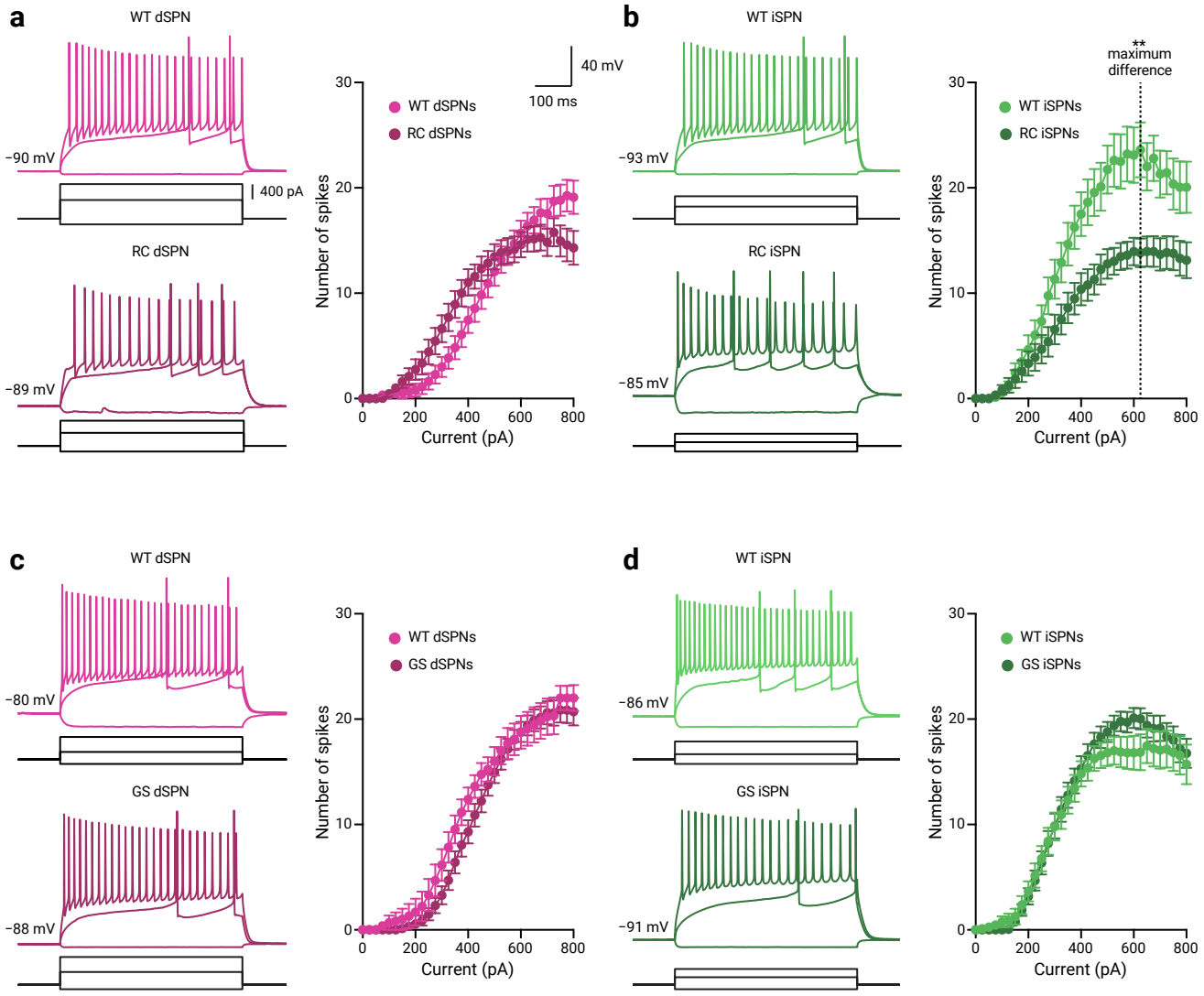
a
WT dSPN
−90 mV
400 pA
RC dSPN
−89 mV
40 mV
100 ms
WT dSPNs
RC dSPNs
Number of spikes
Current (pA)
b
WT iSPN
−93 mV
RC iSPN
−85 mV
**
maximum
difference
WT iSPNs
RC iSPNs
Number of spikes
Current (pA)
c
WT dSPN
−80 mV
GS dSPN
−88 mV
WT dSPNs
GS dSPNs
Number of spikes
Current (pA)
d
WT iSPN
−86 mV
GS iSPN
−91 mV
WT iSPNs
GS iSPNs
Number of spikes
Current (pA)

Figure 2

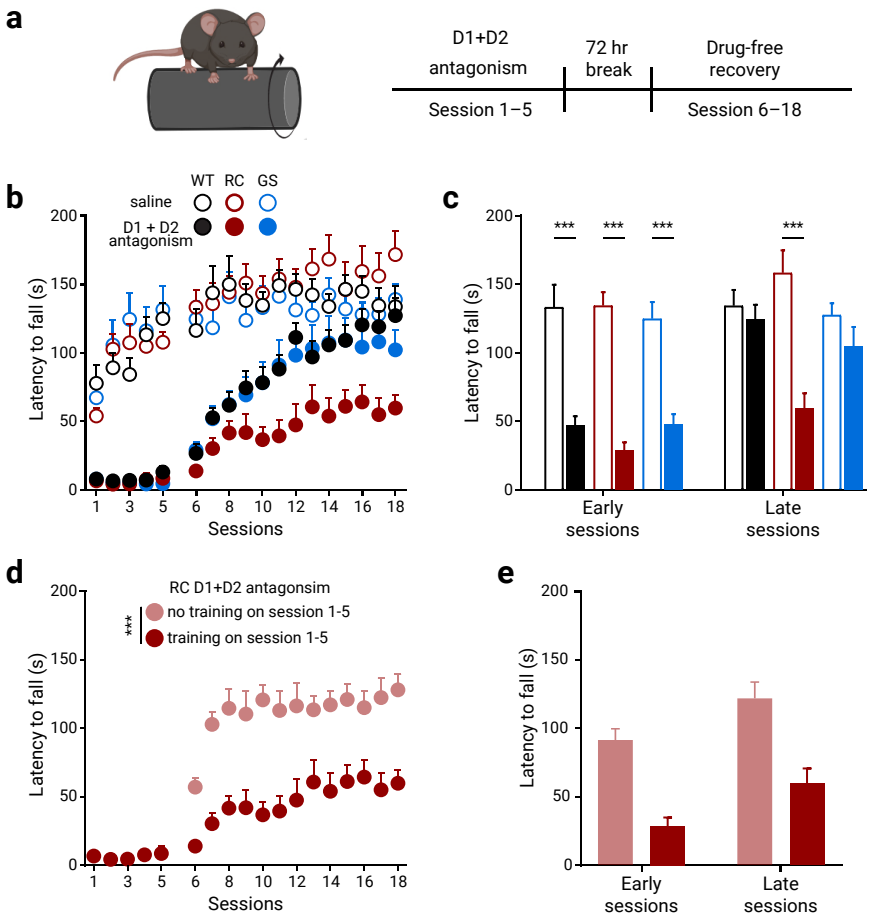
a
D1+D2
antagonism
72 hr
break
Drug-free
recovery
Session 1–5
Session 6–18
b
WT RC GS
saline
D1 + D2
antagonism
Latency to fall (s)
Sessions
c
***
Latency to fall (s)
Early
sessions
Late
sessions
d
RC D1+D2 antagonsim
no training on session 1-5
training on session 1-5
***
Latency to fall (s)
Sessions
e
Latency to fall (s)
Early
sessions
Late
sessions

Figure 3

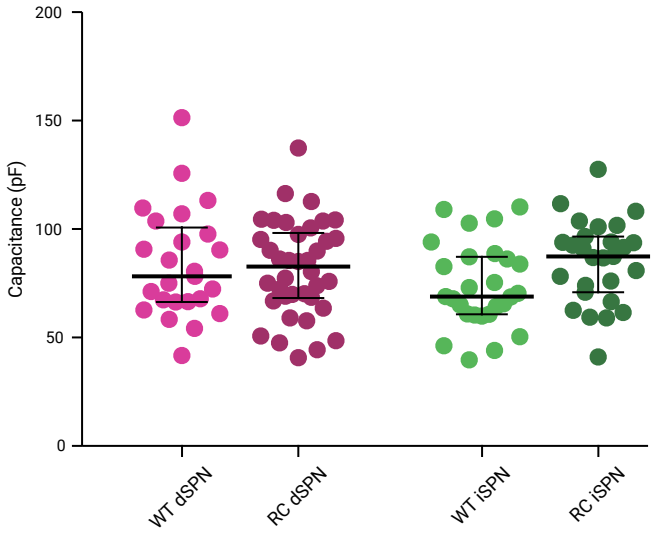

Figure 2–figure supplement 1

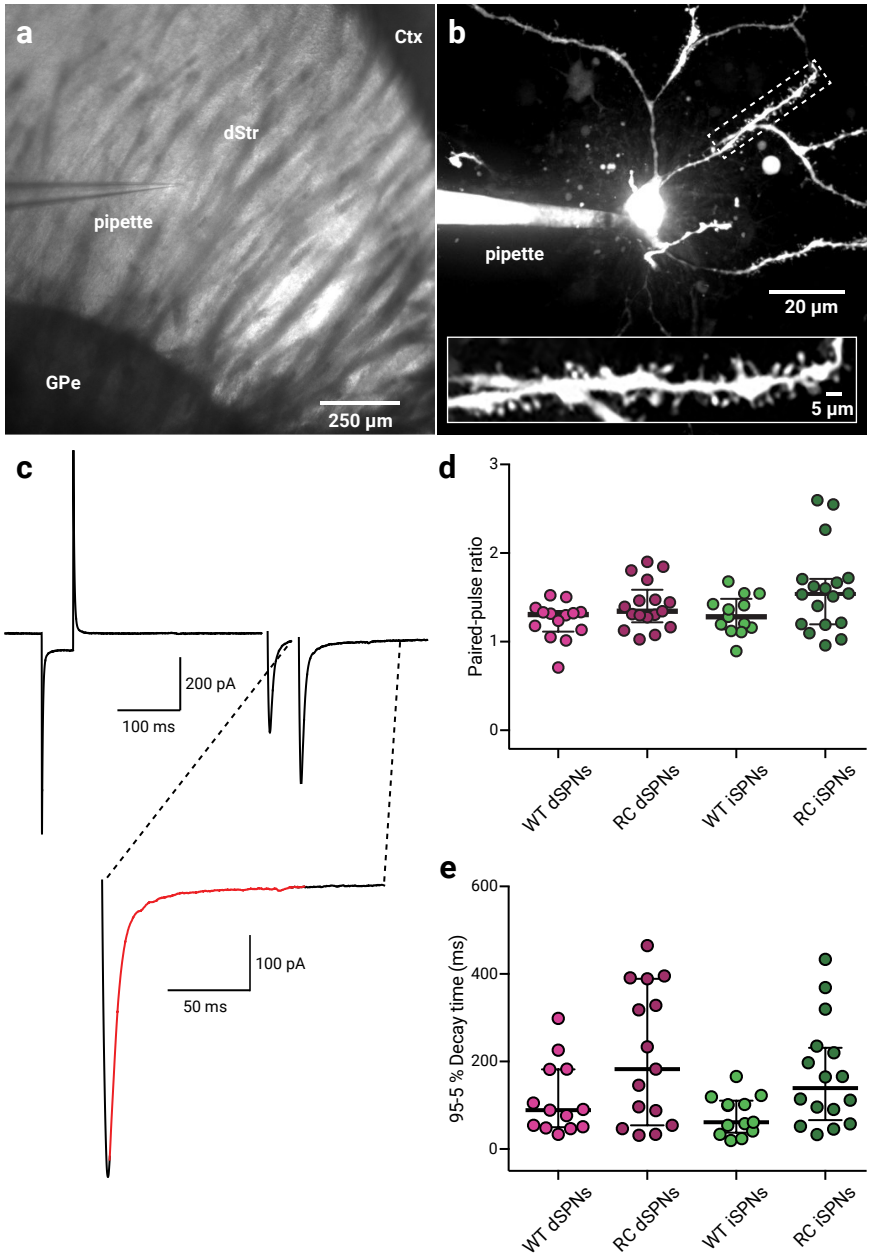

Figure 2–figure supplement 2

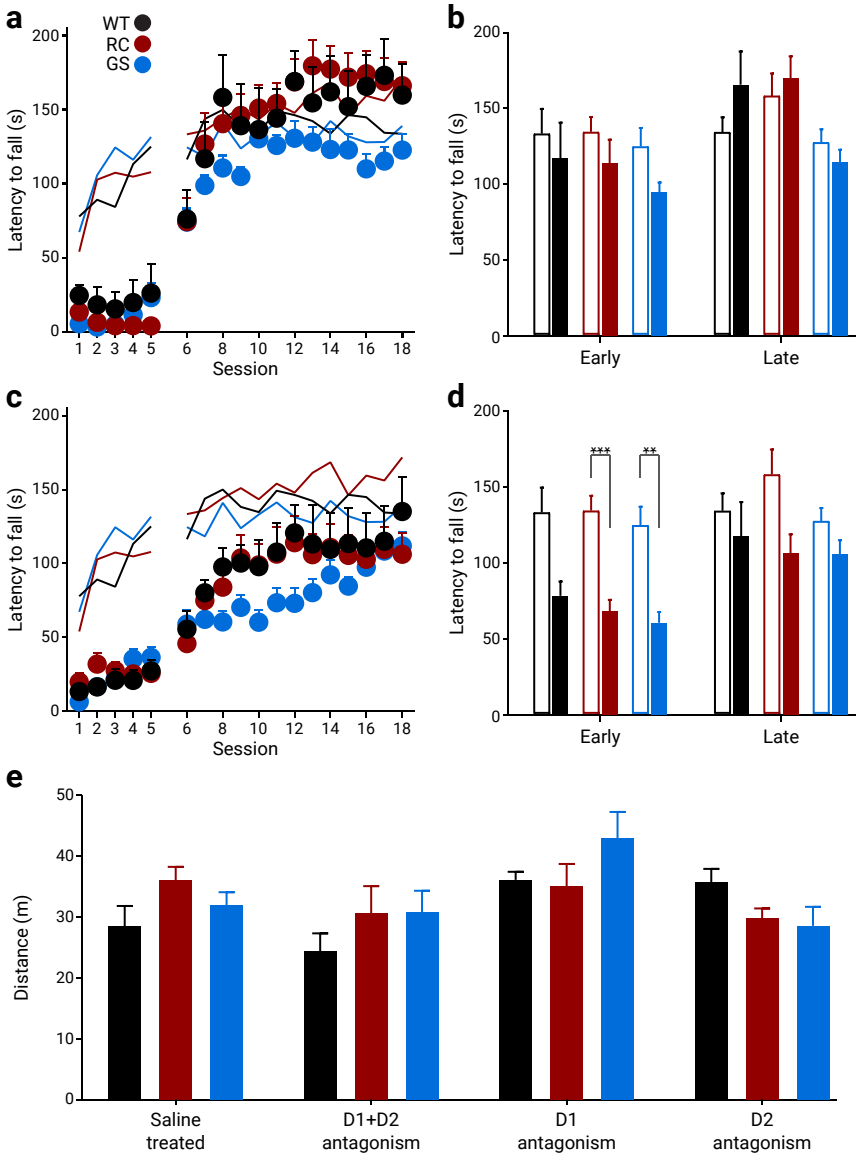

Figure 3–figure supplement 1

Early sessions 6–9

	WT	RC	GS
Saline vs. D1+D2 antagonism	< 0.0001	< 0.0001	0.0007
Saline vs. D1 antagonism	0.9913	0.9593	0.7990
Saline vs. D2 antagonism	0.0549	0.0190	0.0128

	D1 + D2 antagonism	D1 antagonism	D1 antagonism	Saline
WT vs. RC	0.9908	1.0000	1.0000	1.0000
WT vs. GS	1.0000	0.9781	0.9981	1.0000
GS vs. RC	0.9908	0.9936	1.0000	1.0000

Late sessions 16–18

	WT	RC	GS
Saline vs. D1+D2 antagonism	0.9999	<0.0001	0.9842
Saline vs. D1 antagonism	0.5480	1.0000	0.9998
Saline vs. D2 antagonism	1.0000	0.1492	0.9904

	D1 + D2 antagonism	D1 antagonism	D1 antagonism	Saline
WT vs. RC	0.0429	1.0000	1.0000	1.0000
WT vs. GS	0.0952	0.3641	1.0000	1.0000
GS vs. RC	0.4980	0.2661	1.0000	1.0000

Figure 3—table supplement 1